Hindawi
International Journal of Electrochemistry
Volume 2018, Article ID 5919874, 18 pages
https://doi.org/10.1155/2018/5919874

Research Article

An Investigation of Direct Hydrocarbon (Propane) Fuel Cell Performance Using Mathematical Modeling

Bhavana Parackal,[1,2,3] Hamidreza Khakdaman,[4] Yves Bourgault,[5] and Marten Ternan[1,2,6]

[1]*Department of Chemical and Biological Engineering, University of Ottawa, 161 Louis-Pasteur, Ottawa, ON, Canada K1N 6N5*
[2]*Center for Catalysis Research and Innovation, University of Ottawa, 30 Marie-Curie Street, Ottawa, ON, Canada K1N 6N5*
[3]*Clara Pontoppidans Vej 16 1. tv, 2500 Copenhagen, Denmark*
[4]*ExxonMobil Corporation, Process Fundamentals, Global Chemical Research, BTEC-W-3144, 5200 Bayway Drive, TX 77520, USA*
[5]*Department of Mathematics and Statistics, University of Ottawa, 585 King Edward Avenue, Ottawa, ON, Canada K1N 6N5*
[6]*EnPross Incorporated, 147 Banning Road, Ottawa, ON, Canada K2L 1C5*

Correspondence should be addressed to Marten Ternan; ternan@bell.net

Received 1 June 2018; Revised 26 August 2018; Accepted 5 September 2018; Published 2 December 2018

Academic Editor: Sheng S. Zhang

An improved mathematical model was used to extend polarization curves for direct propane fuel cells (DPFCs) to larger current densities than could be obtained with any of the previous models. DPFC performance was then evaluated using eleven different variables. The variables related to transport phenomena had little effect on DPFC polarization curves. The variables that had the greatest influence on DPFC polarization curves were all related to reaction rate phenomena. Reaction rate phenomena were dominant over the entire DPFC polarization curve up to 100 mA/cm^2, which is a value that approaches the limiting current densities of DPFCs. Previously it was known that DPFCs are much different than hydrogen proton exchange membrane fuel cells (PEMFCs). This is the first work to show the reason for that difference. Reaction rate phenomena are dominant in DPFCs up to the limiting current density. In contrast the dominant phenomenon in hydrogen PEMFCs changes from reaction rate phenomena to proton migration through the electrolyte and to gas diffusion at the cathode as the current density increases up to the limiting current density.

1. Introduction

The characteristics of direct hydrocarbon fuel cells (DHFCs) are different than those of hydrogen fuel cells (H2FCs). H2FCs have current densities (reaction rates) that are normally two orders of magnitude greater than DHFCs. Consequently much more research has been performed on H2FCs than on DHFCs. That research has produced many improvements since the initial H2FC experiment performed by Grove [1] in 1839. There are now commercially viable H2FC products available such as materials handling equipment (fork lifts) and fuel cell systems that generate stand-by electrical power. Furthermore, fuel cell powered automobiles can now be purchased in several countries. Perry and Fuller [2] and Eisler [3] have documented some of the history of H2FC development.

In spite of the success enjoyed by H2FCs, there are several factors that favor DHFCs over H2FCs. (a) Existing infrastructure makes hydrocarbon fuels (natural gas, liquefied petroleum gas [LPG] or propane, gasoline, diesel fuel) available almost everywhere. In contrast infrastructure to supply hydrogen fuel does not exist in most places. The cost of manufacturing hydrogen varies with the energy source used to make it. The lowest cost hydrogen is obtained from hydrocarbons (e.g., natural gas) using complex processes involving the steam reforming reaction, high and low temperature water gas shift reactions, and hydrogen purification. More expensive hydrogen can be produced from renewable energy (solar or wind technologies) followed by water electrolysis. (b) Many hydrocarbons can be stored as liquids. The hydrogen storage options are a high pressure gas, a cryogenic liquid

(– 252°C), or a metal hydride. All of the hydrogen storage options are more expensive than liquid storage. (c) The energy density of hydrocarbons is much greater than that of hydrogen. (d) The electrochemical reactions of hydrocarbons have fractional theoretical energy efficiencies of 0.92–0.96 [4]. In contrast that for hydrogen is 0.63 (a combination of 0.83 [4] for the electrochemical energy efficiency and 0.75 for the energy efficiency of the endothermic hydrocarbon steam reforming reaction). Every carbon atom used in a DHFC or in a combination of a process to make hydrogen from hydrocarbons and a H2FC will produce one carbon dioxide molecule. The above difference in their theoretical energy efficiencies indicates that the amounts of carbon dioxide emitted to the atmosphere per unit of energy generated could be smaller for DHFCs than for H2FCs.

Grove performed the first DHFC experiment [5] in 1845. Early research on DHFCs by Becquerel, Jablochkof, Jacques, Borchers, Liebenow and Stresser, Haber, and Hofmann has been documented by Ketelaar [6], who concluded that "fuel cell development had reached a relatively low level during the first 100 years of research". In the 1960s a concentrated research effort on DHFCs was funded in the USA. Results from that program have been reported in three reviews [4, 7, 8]. Sporadic DHFC research has been performed since that time. In our laboratory a phosphoric acid fuel cell was used for experiments that included a commercial low-sulphur diesel fuel at 200°C [9]. Although the current densities were extremely small, the results were encouraging in that steady-state operation was demonstrated for 15 hours with each of four different diesel fuels.

Recently there have been several more encouraging DHFC studies using high temperature direct hydrocarbon solid oxide electrolyte fuel cells (SOFCs). In those studies an internal reforming catalyst layer had been added to the anode catalyst layer. Its purpose was to convert the hydrocarbon to hydrogen before it reached the adjacent anode catalyst layer. Lee and coworkers [10] added a Ni-Fe reforming catalyst layer to an anode layer consisting of NiO–YSZ (yttria stabilized zirconia) in experiments with methane at 750°C. Later [10] they reported a 1000 h continuous fuel cell operation using a ceria coated Ni reforming catalyst in experiments with methane at 610°C. Liu and coworkers [11] added a reforming catalyst layer containing Ni, YSZ, and $BaZr_{(1-X)}\ Y_XO_{(3-\delta)}$ in experiments with iso-octane at 750°C. Zhang et al. [12] showed that direct propane solid oxide fuel cells having electrodes composed of a blend of silver and gadolinium doped ceria maintained a stable performance for 160 h time-on-stream. However experiments with a nickel-gadolinium doped ceria experienced serious deactivation after 40 h of time-on-stream. In all of the above reports on SOFCs the current densities were slightly smaller but of the same order of magnitude as those in H2FCs.

Propane was the fuel chosen for this work for two reasons. Propane is used to provide space heating in rural areas. Therefore the infrastructure for direct propane fuel cells (DPFCs) in rural areas is already in place. Second, the cost for an electrical utility to deliver electrical power in rural areas is much greater than in urban areas even though the price of electrical power in rural and urban areas is similar. Therefore electrical power from a fuel cell system in a rural location may be cost competitive with rural electrical power costs even if it is too expensive for urban areas.

Results with low temperature proton exchange membrane fuel cells (PEMFCs) operating on propane have been less encouraging. Some of the most promising results with propane from the 1960s were obtained with a phosphoric acid electrolyte, Grubb and Michalske [13], and with a hydrofluoric acid electrolyte, Cairns [14]. However, in recent years only a limited amount of work has been reported on DPFCs. Examples are the propane work using Nafion and polybenzimidazole electrolyte membranes by Savadogo and Varela [15] and using a polybenzimidazole membrane by Cheng et al. [16].

Our long-term objective is to seek DPFC characteristics (processing conditions, materials, and equipment configurations) for which the performance of low temperature DPFCs would become competitive with H2FCs. Two steps are necessary to achieve this objective: (a) identifying the limiting phenomena that are responsible for small current densities in DPFCs and (b) identifying the DPFC characteristics that would remove those limitations.

To contribute to the first step, in this work we have used mathematical modeling to examine the effect of several variables that influence DPFC performance. Experiments are always more definitive than models. However there are some variables that are extremely difficult to measure experimentally. An example would be the pressure gradient across the electrolyte layer. In contrast they can sometimes be computed precisely using models. By studying large changes in each of the variables, it should be possible to identify those variables having the greatest potential to improve fuel cell performance.

Mathematical models of fuel cells have been used to describe a wide range of physical, chemical, electrochemical, and mass transfer phenomena. There were several early models. Verbrugge and Hill [17] used dilute solution theory to describe the migration of protons in a fuel cell having a perfluorosulfonate ionomer membrane. Springer et al. [18] developed one of the first models for a hydrogen fuel cell. It predicted a ratio of water flux to proton flux in a Nafion 117 membrane that was consistent with the experimental value. Bernardi and Verbrugge, [19] modeled the transport mechanisms of several species within a PEMFC and found that the diffusion of dissolved gases to the catalyst limited fuel cell performance. Since then models of various complexities have been developed from simple (analytical models), Kim et al. [20], to more complex (mechanistic models), Amphlett et al. [21], and numerical models, Weber and Newman [22]. An extremely large body of literature describing fuel cell models now exists. Some recent reviews are those by Jarauta and Ryzhakov [23], Salomov et al. [24], and Zhang and Jiao [25].

The first mathematical model of a direct propane fuel cell (DPFC) was developed by Psofogiannakis et al. 2006 [26]. It was a one-dimensional computational fluid dynamics (CFD) model. It used a phosphoric acid electrolyte and Pt anode catalyst. Overpotential was found to control fuel cell performance. Subsequently, Khakdaman et al. [27, 28]

developed a two-dimensional mathematical model based on a proton exchange membrane and a Pt anode catalyst. It correctly described the transport of charged species. The electrons (negatively charged) migrated from the anode to the cathode in response to an electrical potential difference. The protons (positively charged) diffused from the anode to the cathode in response to a proton concentration difference. Recently Danilov et al. [29] described a tank-in-series reactor model to describe a direct propane fuel cell.

In this work a two-dimensional direct propane fuel cell model is described, which is an improvement over the models of Khakdaman et al. [28]. A progressive time-stepping method was used to improve convergence so that polarization curves could be predicted over a greater range of current densities. The model was used to investigate an array of variables. The variables were placed in two groups. One group of variables affected mass transport processes. The other group of variables was related to phenomena that occur on the electrochemical catalyst surfaces and therefore affected the reaction rate.

An overview of this work can be summarized in two statements. The main aim of the work described here was to identify the limiting phenomena that might be responsible for the small current densities observed in DPFCs. The novelty of the results reported is that all of the computations were consistent with a single phenomenon limiting the performance of DPFCs.

2. Model Description

The model is based on the following desirable reactions occurring in the fuel cell. The reaction between propane and water at the anode

$$C_3H_8 + 6H_2O = 3CO_2 + 20H^+ + 20e^- \quad \phi_A = 0.136\ \text{V} \quad (1)$$

and the reaction between oxygen in air with protons and electrons at the cathode

$$5O_2 + 20H^+ + 20e^- = 10H_2O \quad \phi_C = 1.229\ \text{V} \quad (2)$$

can be combined to produce the following overall fuel cell reaction.

$$C_3H_8 + 5O_2 = 3CO_2 + 4H_2O \quad \Delta\phi_{CELL} = 1.093 \quad (3)$$

The electrode potentials at 25°C for the anode, ϕ_A, and cathode, ϕ_C, together with the fuel cell potential difference, $\Delta\phi_{CELL}$, [30] are also shown above with their respective stoichiometric reactions.

An undesirable reaction, carbon formation, is thermodynamically possible via an overall fuel cell reaction in which C rather than CO_2 is the product of the reactants in (3) ($\Delta\phi_{CELL}$ = 0.071 V [30]). However, carbon formation has not been generally reported in the fuel cell literature for propane [13–18]. Specifically Grubb and Michalske reported 99.3 % carbon dioxide formation in 44 experiments using a phosphoric acid aqueous electrolyte [13]. Cairns reported 100 % carbon dioxide using a hydrofluoride aqueous electrolyte [14]. Savadogo and Rodriguez [15] reported 100% CO_2 using Nafion and polybenzimidazole polymer electrolytes. Cheng et al. [16] reported that CO and CO_2 were the only products formed using a polybenzimidazole polymer electrolyte. Nevertheless, carbon formation has been reported in fuel cell experiments with longer chain hydrocarbon molecules, n-octane [7], and diesel fuel [9]. In contrast, carbon formation has never been reported in any low temperature direct hydrocarbon fuel cell when methane was the fuel. These experimental results suggest that the hydrocarbon chain length of the fuel molecule determines whether or not carbon is formed in a direct hydrocarbon fuel cell. Since carbon formation was not reported in the fuel cell experiments with propane, its formation was not included in this model.

The modeling domain of the DPFC consisted of an anode catalyst layer (ACL), an electrolyte (membrane) layer (ML), and a cathode catalyst layer (CCL). Zirconium phosphate ($Zr(HPO_4)_2 \bullet H_2O$ or ZrP) was the proton conducting material or the electrolyte used in the model. The membrane layer consisted of solid ZrP that filled the pores of porous polytetrafluoroethylene (PTFE) [31]. The catalyst layer was composed of carbon supported platinum (Pt) catalyst and ZrP electrolyte. Interdigitated flow fields (IDFF) were used both for the anode and cathode. One of the flow channels in the flow field was used for the reactants and the other for the products. The catalyst layer was composed of three phases, i.e., the gas phase, the solid electrolyte phase, and the solid catalyst phase.

Khakdaman's mathematical description [28] of a fuel cell formed the starting point for the model used here. Four conservation equations were used in the model: the conservation of momentum, total mass, total charge, and individual component species including a reaction term. The governing equations of the model included (a) the conservation of mass in the gas phase, (b) the Ergun equation, (c) the Butler-Volmer equation (used to calculate the reaction rate at the anode and cathode), and (d) conservation equations for water and for protons in the electrolyte phase and in the two catalyst layers.

The governing equations are shown below:

(a) Conservation of mass in the gas phase

$$\nabla \bullet \left(\varepsilon_G\ \rho_G\ \mathbf{u}\right) + \sum_i^n \frac{\nu_i MW_i j}{zF} = 0 \quad (4)$$

Mass conservation in the gas phase is described by (4). Electrochemical reactions in the gas phase can be either a source or sink. They are described by the second term in the equation.

(b) Conservation of momentum in the gas phase

$$-\nabla P = 150 \left[\frac{\mu_G \left(1-\varepsilon_G\right)^2}{D_G^2 \varepsilon_G^2.}\right] \mathbf{u} \quad (5)$$

The Ergun equation in linear form is shown in (5). Since the catalyst layers are packed beds, the Ergun equation can be used to calculate the pressure profiles in the gas phase. The magnitude of the quadratic term in the Ergun equation is much smaller than that of the linear term at the conditions used in this study. The velocity and pressure profiles in the gas

phase of the catalyst layers were obtained by simultaneously solving (4) and (5).

(c) Conservation of noncharged species in the gas phase

$$\nabla \bullet (\varepsilon_G\, c_G\, \mathbf{u}\, y_i) - \nabla \bullet (\varepsilon_G\, c_G\, D_i\, \nabla\, y_i) + \frac{\nu_i j}{zF} = 0 \quad (6)$$

$i = C_3H_8$ and CO_2 for the anode, and O_2 and H_2O for the cathode.

Equation (6) was used to obtain mass balances for each of the individual gas phase species. Separate terms for convection, diffusion, and reaction are included in (6).

(d) Conservation of species in the electrolyte phases of the membrane and catalyst layers

(d1) For water

$$\begin{aligned} .-\nabla \bullet \left(c_{ELY}\left(B'_{H2O-H2O} - B'_{H2O-H+}\right)\nabla x_{H+}\right) + \nabla \\ \bullet \left(c_{ELY} B'_{H2O-H+} \frac{F\, x_{H+}}{RT} \nabla \phi_{ELY}\right) - \frac{j}{zF} = 0 \end{aligned} \quad (7)$$

(d2) For protons

$$\begin{aligned} \nabla \bullet \left(c_{ELY}\left(B'_{H+-H+} - B'_{H+-H2O}\right)\nabla x_{H+}\right) + \nabla \\ \bullet \left(c_{ELY} B'_{H+-H+} \frac{F x_{H+}}{RT} \nabla \phi_{ELY}\right) + \frac{j}{zF} = 0 \end{aligned} \quad (8)$$

Mass balances for water and protons in the electrolyte phases of the catalyst and membrane layers were obtained using (7) and (8). Concentrated solution theory through the generalized Maxwell Stefan equations was used to describe diffusion. The B' terms are composition-dependent parameters obtained using the methodology given by Khakdaman et al. [31] that include the diffusivities for the various mobile species.

(e) Butler-Volmer equation at the anode

$$j_A = j_A^0 A_{Pt}\left(\exp\left(\frac{\alpha_A F \eta_A}{RT}\right) - \exp\left(\frac{-\alpha_A F \eta_A}{RT}\right)\right) \quad (9)$$

$$\begin{aligned} \text{where, } j_A^0 = \left(j_{C3\ Ox}\right)^{0ref}\left(\frac{p_{C3}}{\left(p_{C3}\right)^{ref}}\right) \\ \cdot \exp\left(\frac{\left(\Delta G_{C3Ox}\right)^{\pm}}{R}\left(\frac{1}{T^{ref}} - \frac{1}{T}\right)\right) \end{aligned} \quad (10)$$

The rate of production of protons at the anode, j_A, is described by the Butler-Volmer equation in (9) and has a positive value. The exchange current density used in (9) is given in (10). It is a function of both the operating temperature and the partial pressure of the propane reactant. The anode reference exchange current density $(j_{C3\text{-}Ox})^{0\text{-ref}}$ term includes the reaction rate constant for the anode reaction.

(f) Butler-Volmer equation at the cathode

$$j_C = j_C^0 A_{Pt}\left(\exp\left(\frac{\alpha_C F \eta_C}{RT}\right) - \exp\left(\frac{-\alpha_C F \eta_C}{RT}\right)\right) \quad (11)$$

$$\begin{aligned} \text{where, } j_C^0 = \left(j_{O2\ Rd}\right)^{0ref}\left(\frac{p_{O2}}{\left(p_{O2}\right)^{ref}}\right) \\ \cdot \exp\left(\frac{\left(\Delta G_{O2Rd}\right)^{\pm}}{R}\left(\frac{1}{T^{ref}} - \frac{1}{T}\right)\right) \end{aligned} \quad (12)$$

The rate of consumption of protons at the cathode is described by the Butler-Volmer equation in (11) and has a negative value. The exchange current density used in (11) is given in (12). It is a function of the operating temperature and the partial pressure of the oxygen. The cathode reference exchange current density $(j_{O2-Rd})^{0-ref}$ term includes the reaction rate constant for the cathode reaction.

(g) The overpotentials at the anode, η_A, and cathode, η_C, are given by (13) and (14), respectively.

$$\begin{aligned} \eta_A &= \Delta\phi_A - \Delta\phi_A^{EQ} \\ &= \left(\phi_{Pt\text{-}A} - \phi_{ELY\text{-}A}\right) - \left(\left[\phi_{Pt\text{-}A}\right]^{EQ} - \left[\phi_{ELY}\right]^{EQ}\right) \end{aligned} \quad (13)$$

$$\begin{aligned} \eta_C &= \Delta\phi_C - \Delta\phi_C^{EQ} \\ &= \left(\phi_{Pt\text{-}C} - \phi_{ELY\text{-}C}\right) - \left(\left[\phi_{Pt\text{-}C}\right]^{EQ} - \left[\phi_{ELY}\right]^{EQ}\right) \end{aligned} \quad (14)$$

In the work described here Khakdaman's model [28] was improved by adding a progressive time-stepping method within the iteration loop that contained all the governing equations. The modified iteration loop is shown on the right-hand side of the modeling flow chart shown in Figure 1. This progressive time-stepping method speeds up the computation of the polarization curve by doing a fixed number, N, of time-steps (N=19 for Φ_{Ag} - $\Phi_{Ni} \geq 0.793$ and N=39 for Φ_{Ag} - $\Phi_{Ni} < 0.793$). After the N time-steps, Φ_{Ag} - Φ_{Ni} is decremented by a small value to proceed further along the polarization curve instead of completing the time loop before changing Φ_{Ag} - Φ_{Ni}. Φ is the equilibrium potential of the cathode, Ag, and anode, Ni, electrodes, respectively. The progressive time-stepping method included a local overpotential cut-off value at the anode and cathode of 0.432 V. Any grid point having an overpotential larger than 0.432 V was forced to take the value 0.432 V. This occurred at very few points in the anode and cathode. The value of 0.432 V was set by trial and error to limit the impact of this cut-off.

Figure 2 shows the fuel cell performance predicted by the DPFC model with and without the progressive time-stepping method in the iteration loop. The figure represents the polarization curve for a DPFC at 150°C and 1 atm. It is a plot of cell potential difference, $\Delta\Phi_{cell}$ (V), versus current density (mA/cm^2). The progressive time-stepping method improved convergence and thereby is seen to extend the polarization curve to larger current densities. Specifically, convergence occurred up to a current density of 106 mA/cm^2 for the model with the progressive time-stepping method in comparison to 51 mA/cm^2 for the nonprogressive method.

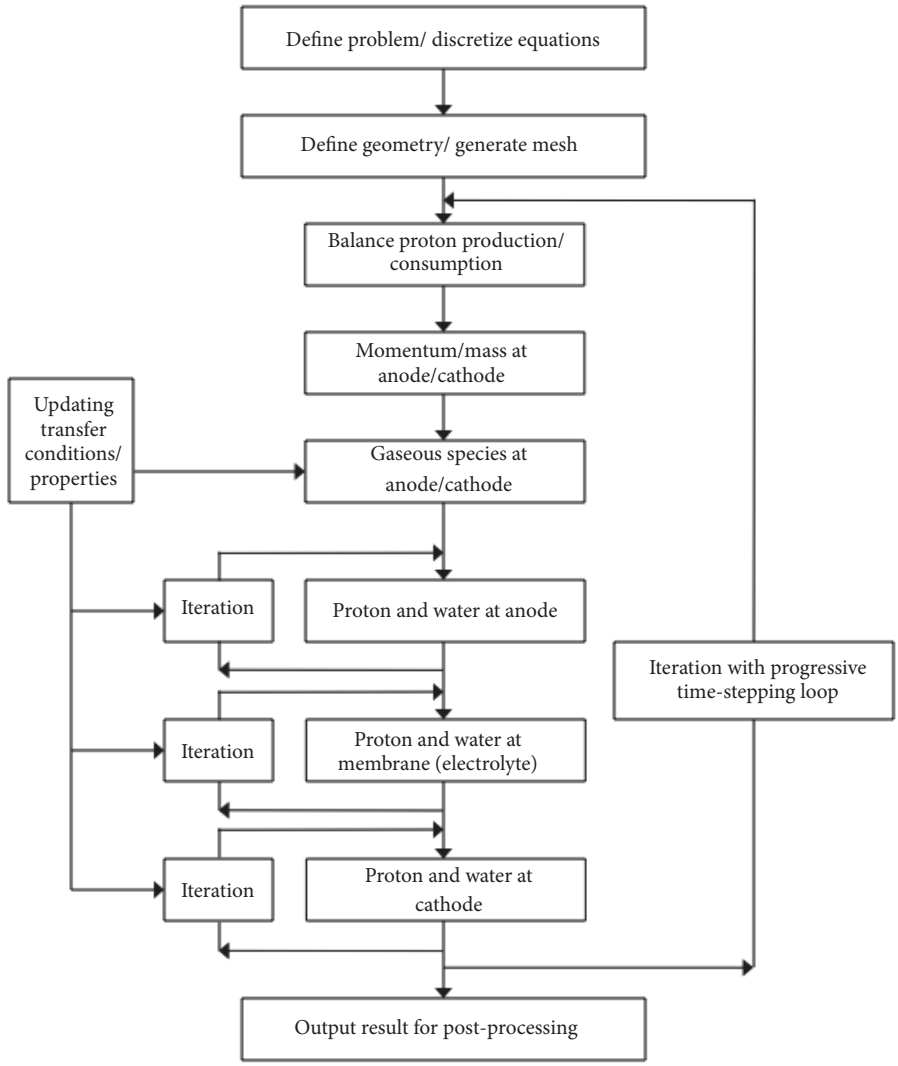

Figure 1: The computational procedure with the time-stepping progressive iteration loop [2].

The DPFC polarization curve shown in Figure 2 resulting from the progressive time-stepping method was used as the reference case. The reference case polarization curve was compared to the other polarization curves that were obtained at the variety of conditions investigated in this study. The maximum current density at which convergence occurred was different for each variable investigated. Values for the various variables used in the DPFC model are shown in Table 1. Design and operational variables, other than those in Table 1, were the same as the ones reported by Khakdaman et al. [28].

Several assumptions were made during the development of the model. As explained already, one of the assumptions was that no solid carbon was formed from the propane feedstock and that all of the carbon atoms in the feedstock left the fuel cell in the form of carbon dioxide. Also it was assumed that no degradation in fuel cell performance occurred by any other phenomena (e.g., CO poisoning of Pt anode catalyst). Several properties, diffusivities, proton conductivity in the electrolyte, electrical resistivity in the membrane, and charge transfer coefficients were assumed to have the values shown in Table 1. It was assumed that concentrated solution theory could be used to describe the behavior of species in the electrolyte. It was assumed that the mole fraction in the electrolyte could be calculated by assuming that each proton was associated with one water molecule rather than multiple water molecules. It was assumed that there was no cross-over of propane from the anode catalyst layer to the cathode catalyst layer.

3. Results and Discussion

Polarization curves are plots of potential difference between the anode and cathode, $\Delta\Phi_{cell}$, (V) versus current density (mA/cm^2). The operating conditions were 150°C and 1 atm. For hydrogen PEMFCs polarization curves can be divided into different regions. In each region a different mechanism

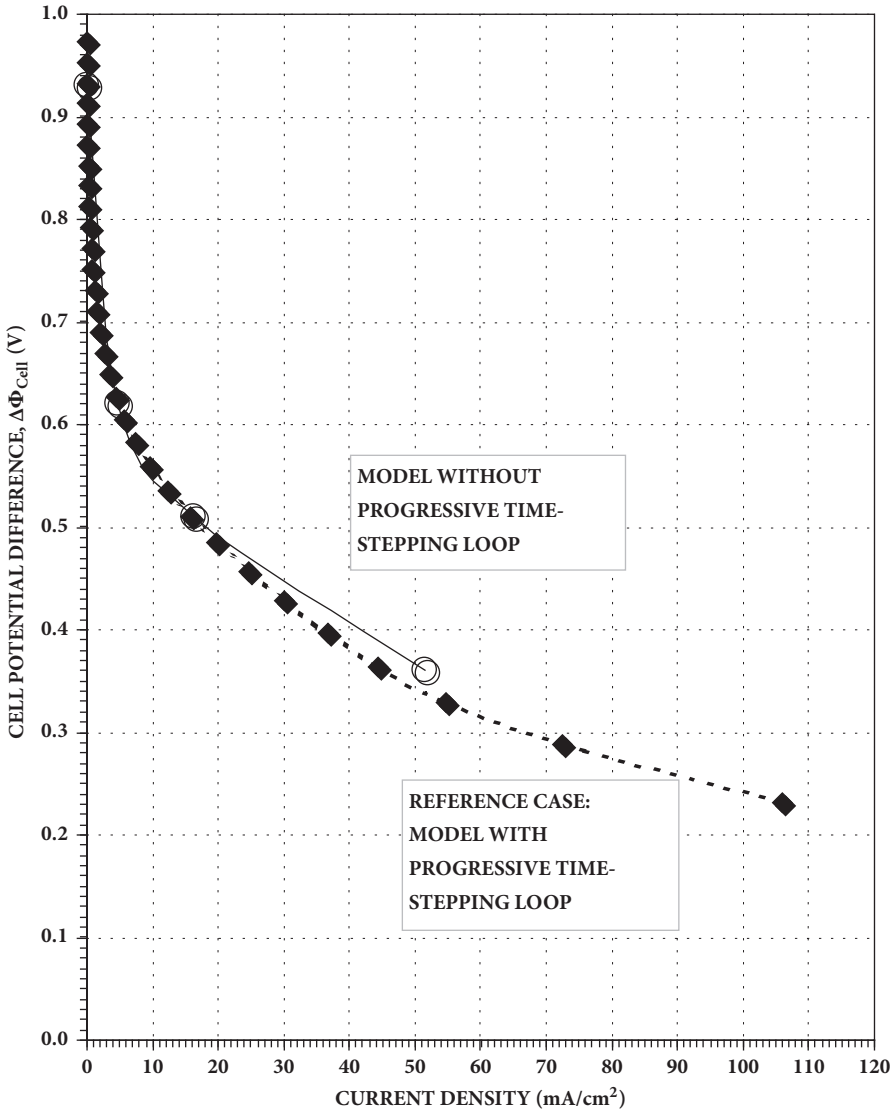

Figure 2: The effect of progressive and nonprogressive time-stepping loops on the polarization curve for a direct propane fuel cell model (DPFC) at 150°C and 1 atm. The above two cases were represented by the following symbols: (i) open circles: model without a progressive time-stepping loop, and (ii) solid diamonds: model with a progressive time-stepping loop.

controls the performance of the fuel cell. At small current densities the reaction rate is controlled by the electrode overpotential, η. At intermediate current densities Ohmic losses (proton transport across the electrolyte) control the reaction rate. Finally at high current densities, mass transfer limitations (e.g., oxygen transport through liquid water at the cathode of a PEM fuel cell) may control the reaction rate. When the value of a variable was changed in this study, its effect on the polarization curve was used to indicate its impact on the performance of the fuel cell. In the investigation reported here, all the variables were held constant (at the same values as in the reference case) except for the variable being studied.

The first variable investigated was the anode reference exchange current density, $(j_{C3\text{-}Ox})^{0\text{-}ref}$. The reference exchange current density represents the electrocatalytic properties of the catalyst used in the membrane electrode assembly (MEA) of the fuel cell. It includes the rate constant for the electrocatalytic reaction. Changes in the reference exchange current density reflect changes in the rate constant. The effect of the anode reference exchange current density on the overall performance of a direct propane fuel cell (DPFC) is shown in Figure 3. A current density of 40 mA/cm^2 was chosen to compare the results obtained in Figure 3. As the anode reference exchange current density $(j_{C3\text{-}Ox})^{0\text{-}ref}$ increased by four orders of magnitude (i.e., from 0.07 to 7 to 700 mA/m^2), the potential difference between the fuel cell electrodes also increased (i.e., from 0.38 to 0.72 to 1.04 V, respectively). These data indicate that the anode reference exchange current density (and therefore the anode catalyst composition) has a large impact on fuel cell performance.

The Butler-Volmer equation for the anode is shown in (9). The anode exchange current density, j_A^0, like the anode reference exchange current density, is related to the rate constant

Table 1: Operational, electrochemical, and design parameters of the reference case of the DPFC model (see [28]).

Parameter	Value
Temperature, T	423 K
Pressure, P	1 atm
Propane inlet molar flow rate, m_P	$8x10^{-6}$ gmol s^{-1}
Propane inlet mole fraction, y_{Pinput}	0.1
Reference exchange current density at the anode, $j_{0AN\text{-}ref}$	$7x10^{-5}$ A $m^{-2}_{Pt\text{-}catalyst}$
Reference exchange current density at the cathode, $j_{0CA\text{-}ref}$	$3x10^{-8}$ A $m^{-2}_{Pt\text{-}catalyst}$
Proton diffusivity coefficient in the electrolyte (ZrP) phase, $D_{H+\text{-}ZrP}$	$3x10^{-9}$ m^2 s^{-1}
Water diffusivity coefficient in the electrolyte (ZrP) phase, $D_{H2O\text{-}ZrP}$	$2x10^{-8}$ m^2 s^{-1}
Proton-water diffusivity coefficient, $D_{H2O\text{-}H+}$	$1.32x10^{-8}$ m^2 s^{-1}
Proton conductivity in the electrolyte (membrane) layer, σ_{ELY}	5 S m^{-1}
Specific surface area of anode and cathode carbon catalyst support, A_{CAT},	200 $m^2_{catalyst}$ $g^{-1}_{catalyst}$
Land width, L_w	4.4 mm
Anode and cathode thickness, Th_A, Th_C	300 μm
Membrane thickness, Th_M	100 μm
Fluid channels width in bi-polar plates	0.2 mm
Electrical resistivity in membrane, R_{PTFE}	$1x10^{16}\Omega$ m
Charge transfer coefficients, α_A and α_C	1

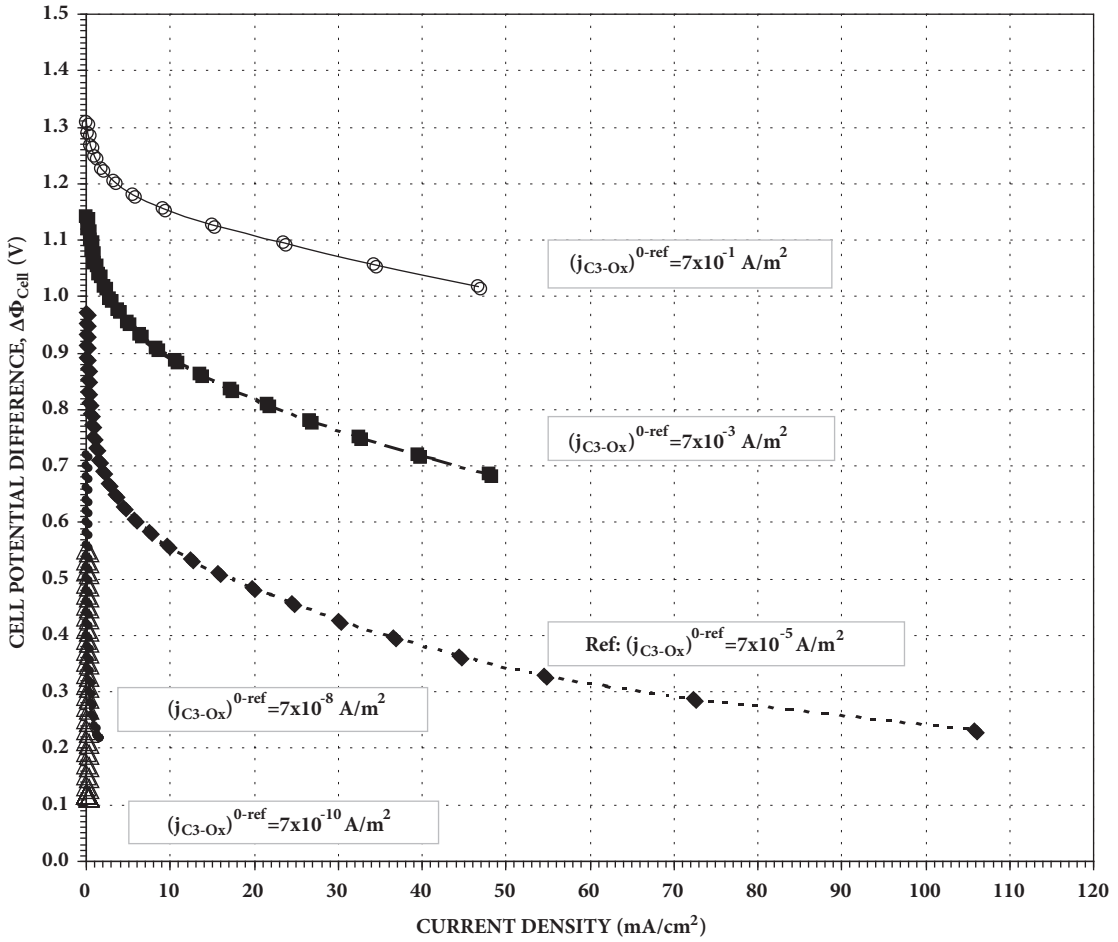

Figure 3: The effect of the anode reference exchange current density, $(j_{C3\text{-}Ox})^{0\text{-}ref}$ (A/m^2), on the polarization curve for a direct propane fuel cell model (DPFC) at 150°C and 1 atm. The values of $(j_{C3\text{-}Ox})^{0\text{-}ref}$ (A/m^2) for the above five cases were represented by the following symbols: (i) open circles: $7x10^{-1}$ A/m^2, (ii) solid squares: $7x10^{-3}$ A/m^2, (iii) solid diamonds: $7x10^{-5}$ A/m^2 (reference case), (iv) solid circles: $7x10^{-8}$ A/m^2, and (v) open triangles: $7x10^{-10}$ A/m^2. All the other parameters were the same as the reference case mentioned in Table 1.

(k) for the electrochemical reaction. Therefore changing the catalyst composition can change the rate constant and thereby change both the reaction rate and the current density.

For hydrogen-oxygen fuel cells with acidic membranes and platinum electrodes, the anode exchange current density can be five to seven orders of magnitude greater than the cathode exchange current density [32]. Nevertheless anode composition does have an effect. For example, with hydrogen fuel cells changing the composition of the anode from Pt to Ir can cause a change in the anode exchange current density of almost two orders of magnitude [33]. Therefore anode composition (and therefore anode exchange current density) does cause a difference in performance as indicated in Figure 3.

Direct hydrocarbon fuel cells are different than hydrogen fuel cells. For example, with platinum electrodes the anode exchange current density for ethylene and the cathode exchange current density for oxygen are virtually the same. [33]. Similarly our previous work with propane-air fuel cells [27] indicated that the exchange current density at the anode was somewhat less than that at the cathode. These examples indicate that the difference between the anode and cathode exchange current densities is much larger in hydrogen fuel cells than in direct hydrocarbon fuel cells.

The review by Davydoda et al. [34] shows that the beginning of life performance with anion exchange membranes approaches that of proton exchange membranes. It is now known that the performance of platinum anode catalysts with anion exchange membranes is much worse than with proton exchange membranes. Experiments in anion exchange membrane fuel cells with several non-platinum anode catalysts indicated that the results varied with anode catalyst composition. A Ni-Mo anode catalyst was one of the best non-platinum catalysts [34]. It is apparent that the family of fuel cells having anion exchange membranes is similar to direct hydrocarbon fuel cells in that the anode catalyst composition has a large effect on fuel cell performance in both of them.

There are some indications that it may be possible to improve the performance of the anode catalysts and therefore improve the performance of the anode exchange current density, in direct hydrocarbon fuel cells. We have performed density functional theory computations for anode electrodes having different compositions [32, 35]. The base calculation was made with an anode electrode composition of pure nickel, which is used in the anodes of alkaline fuel cells. Subsequently calculations were performed with copper-nickel alloys. The activation energy of some alloy catalyst was found to be one-third of the value of a pure nickel electrode [35].

The effect of the cathode reference exchange current density, $j(_{O2\text{-}Rd})^{0\text{-}ref}$, on the performance of the DPFC is shown in Figure 4. At a current density of 40 mA/cm^2, as the cathode reference exchange current density, $j(_{O2\text{-}Rd})^{0\text{-}ref}$, increased by two orders of magnitude (i.e., from 3 to 300 nA/m^2), the potential difference between the fuel cell electrodes also increased (i.e., from 0.38 to 0.54 V, respectively). From these observations, it was clear that the cathode reference exchange current density (and therefore the cathode catalyst composition) also had a large effect on fuel cell performance but not as much as the anode reference exchange current density.

Like the anode composition mentioned above, changing the cathode composition can affect the cathode exchange current density. Numerous studies have been performed in which the cathode catalyst composition has been changed in order to improve the oxygen reduction reaction at the cathode. Wang et al. [36] incorporated polyhedron nanocrystals into the cathode catalyst layer and reported improved performance. Liang et al. reported superior performance with intermetallic metal-platinum (metal = Fe, Co, Cu, Ni) nanocrystals [37] as the cathode catalyst. Chandran et al. [38] used Pd alloys. Liu et al. [39] reported that a Pt-Co alloy was superior to pure Pt, Pt-Ni, and Pt-Fe alloys. Kiani et al.[40] reviewed a variety of non-platinum cathode catalysts. The review by Higgins and Chen [41] indicated that the most promising catalyst materials are prepared by the pyrolysis of transition metal–nitrogen–carbon complexes. In each of these cases a change in the cathode catalyst composition (which affects cathode exchange current density) caused a change in performance.

The catalyst layer thickness in both the anode (Th_A) and cathode (Th_C) are other variables that could also affect the fuel cell performance, because they affect the volume of the catalyst per unit face area available for the reaction. Both layers had the same thickness ($Th_A = Th_C$) in the polarization curves shown in Figure 5. At a current density of 40 mA/cm^2, as the thickness of the catalyst layers (Th_A and Th_C) was increased by a factor of two (i.e., from 0.2 to 0.4 mm), the potential difference between the fuel cell electrodes also increased (i.e., from 0.335 to 0.41 V corresponding to 23%). From these observations, it was evident that catalyst layer thickness did have an impact on the overall performance of the DPFC. It should be noted that the catalyst layer thickness only increased by a factor of two and not by the orders of magnitude increases made for the exchange current densities.

Darab et al. [42] performed hydrogen fuel cell experiments in which the thickness of the cathode catalyst was varied. In their work they kept the total Pt loading constant. They found that the initial electrochemical performance was independent of catalyst layer thickness. The results in Figure 5 were obtained with the Pt catalyst content increasing with increasing thickness of the catalyst layer. The results of constant performance with constant total Pt that were obtained by Darab et al. would appear to be consistent with the results in Figure 5 where the performance improved as the total Pt content increased (total Pt content increased with increasing catalyst layer thickness).

The variable investigated in Figure 6 was the membrane layer thickness (Th_M) of the fuel cell. Its effect can be seen when the Ohmic loss is rate controlling, normally the middle part of a hydrogen polarization curve. At a current density of 40 mA/cm^2, as the thickness of the electrolyte (membrane) layer was increased by a factor of five, from 100 to 532 μm, the potential difference between the fuel cell electrodes decreased from 0.38 to 0.35 V. Furthermore,

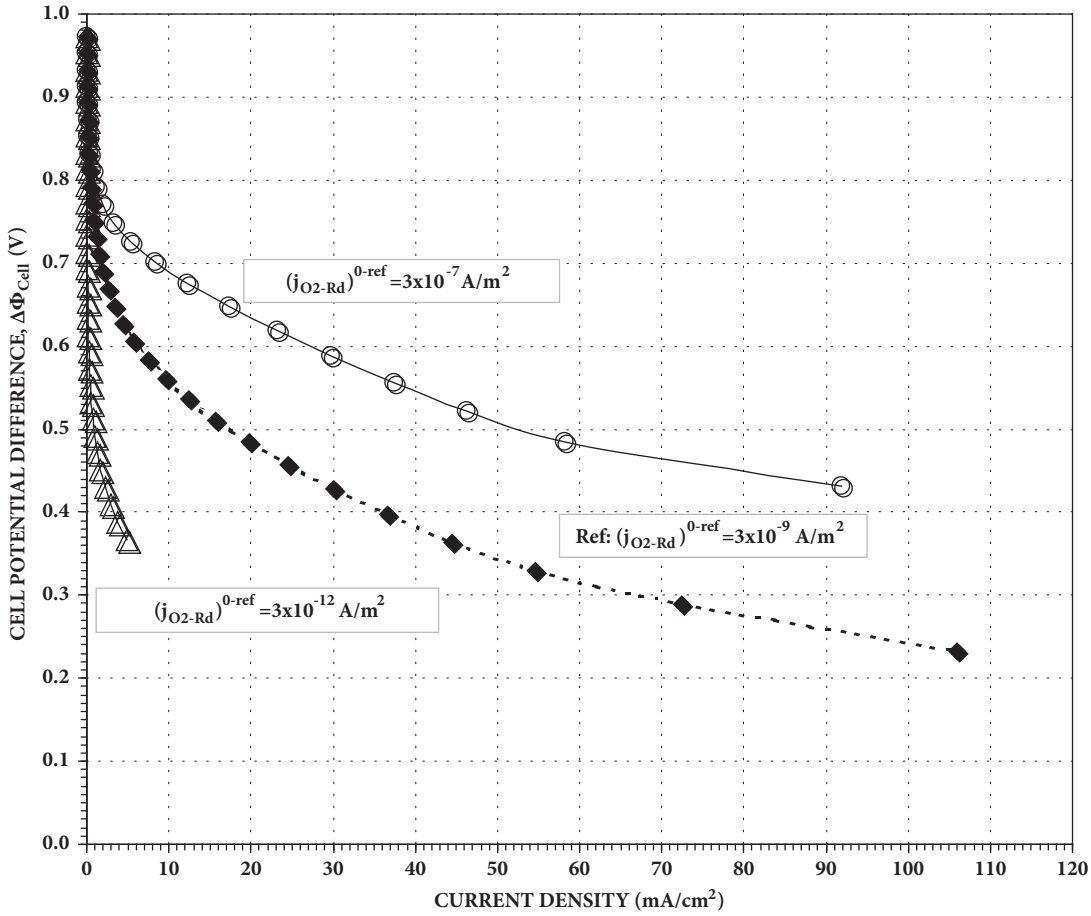

FIGURE 4: The effect of the cathode reference exchange current density, $j(_{O2\text{-}Rd})^{0\text{-}ref}$ (A/m^2), on the polarization curve for a direct propane fuel cell (DPFC) model at 150°C and 1 atm. The values of $j(_{O2\text{-}Rd})^{0\text{-}ref}$ (A/m^2) for the above three cases were represented by the following symbols: (i) open circles: 3x10^{-7} A/m^2, (ii) solid diamonds: 3x10^{-9} A/m^2 (reference case), and (iii) open triangles: 3x10^{-12} A/m^2. All the other parameters were the same as the reference case mentioned in Table 1.

when the membrane layer thickness (Th_M) was increased from 25 to 100 μm, there were no significant changes in potential difference. From these observations, it was evident that the resistance caused by the membrane layer thickness did not have a significant effect on the fuel cell performance in comparison to other variables. De Caluwe et al. [43] measured the properties of Nafion membranes of varying thickness. They found that the relationship between the water content and the proton conductivity was nonlinear. They did not report any measurements of fuel cell performance.

The proton conductivity (σ_{ELY}) of the membrane (electrolyte) layer was also investigated. The term proton conductivity refers to the migration of protons caused by an electrical potential gradient. It is different than proton diffusivity that will be discussed next. The effect of the membrane layer proton conductivity (σ_{ELY}) on the fuel cell performance can be seen in Figure 7. At a current density of 40 mA/cm^2, when the proton conductivity of the electrolyte (membrane) layer (σ_{ELY}) was increased from 5 S/m to 1x10^{20} S/m, there was no significant change in fuel cell performance. Therefore the membrane layer proton conductivity was not rate limiting and had almost no effect on the performance of the DPFC.

Zaidi [44] used hydrogen fuel cell performance to compare two membranes having different proton conductivities. The Hyflon membrane had a greater proton conductivity than the Nafion membrane. It had superior fuel cell performance at current densities greater than 500 A/m^2. However at small current densities, such as the values in Figure 7, the fuel cell performance with the two different membranes was essentially the same. Thus Zadi's experimental results were consistent with the computational results shown in Figure 7 indicating that proton conductivity had no effect at small current densities.

Proton diffusivity in the electrolyte phase was also investigated. The term proton diffusivity refers to the diffusion of protons caused by a proton concentration gradient. The effect of proton diffusivity on the fuel cell performance is shown in Figure 8. When the proton diffusion coefficient ($D_{H+\text{-}ZrP}$) increased by more than an order of magnitude (from 3x10^{-10} to 7x10^{-9} m^2/s), there was minimal change over the range

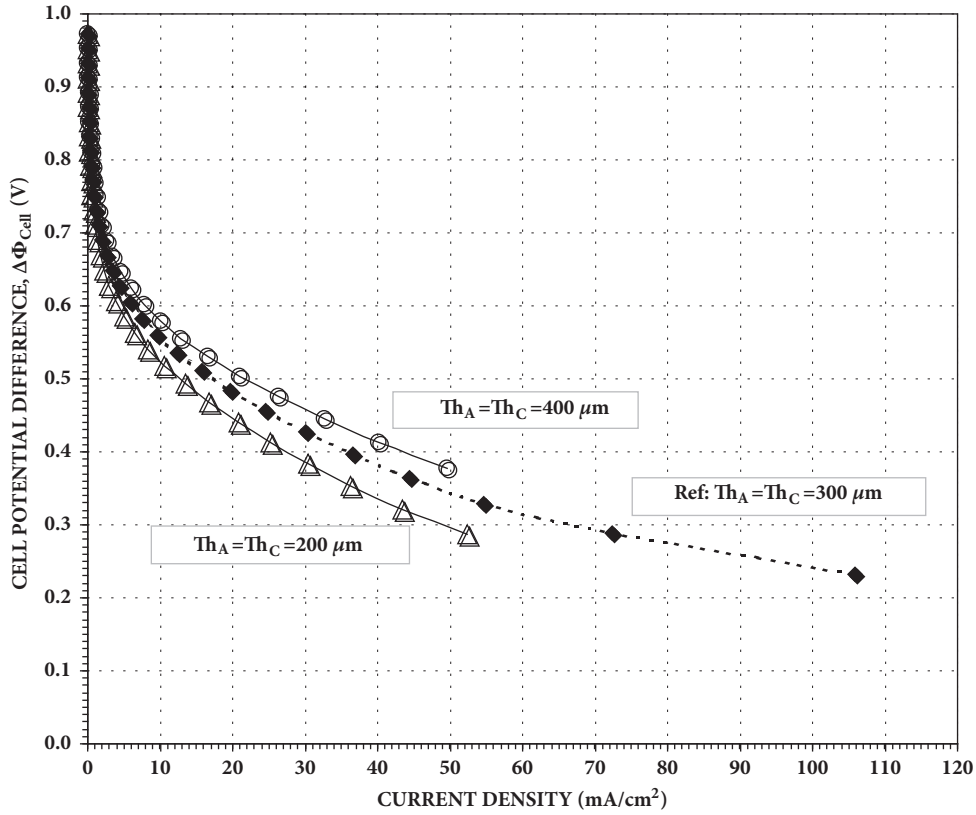

FIGURE 5: The effect of the anode and cathode catalyst layer thickness, $Th_A = Th_C$ (μm), on the polarization curve for a direct propane fuel cell (DPFC) model at 150°C and 1 atm. The values of $Th_A = Th_C$ (μm) for the above three cases were represented by the following symbols: (i) open circles: 400 μm, (ii) solid diamonds: 300 μm (reference case), and (iii) open triangles: 200 μm. All the other parameters were the same as the reference case mentioned in Table 1.

of variables investigated. From these observations, it was concluded that the proton diffusion coefficient did not affect fuel cell performance when compared to the other variables.

Water diffusivity in the electrolyte phase was also investigated. Its effect on the fuel cell performance is shown in Figure 9. When the water diffusion coefficient ($D_{H2O\text{-}ZrP}$) changed from $2x10^{-10}$ to $2x10^{-2}$ m^2/s, there was no noticeable change at any position in the polarization curve. Therefore it was evident that changes to the water diffusion coefficient had virtually no effect on the overall performance of the DPFC.

The propane inlet mole fraction in the feed (y_{Pinput}) (which is related to the reactants' ratio of propane to water) to the fuel cell was also investigated. Its influence on the overall performance of the fuel cell is shown in Figure 10. At a current density of 20 mA/cm^2, as the propane inlet mole fraction increased (from 0.08 to 0.8), the potential difference between the fuel cell electrodes also increased (i.e., from 0.45 to 0.65 V). Increasing the propane inlet mole fraction increases the propane partial pressure and thereby increases the propane adsorption rate. That would be one explanation for its comparatively large impact on the fuel cell performance.

The propane inlet molar flow rate was also investigated. Its effect on the overall performance of the fuel cell is shown in Figure 11. At a current density of 40 mA/cm^2, as the propane inlet molar flow rate (m_P) increased by a factor of eight, from $2x10^{-6}$ to $16x10^{-6}$ gmol/s, the potential difference between the fuel cell electrodes also increased from 0.36 to 0.40 V. Therefore, the propane inlet molar flow rate had little impact on the propane partial pressure, as shown in Figure 11. The propane inlet molar flow rate will only have an effect if it changes the propane mole fraction. It is known that changing the propane inlet mole fraction, shown in Figure 10, had a significant impact on the propane partial pressure. Since the current densities with all the DPFC polarization curves discussed in this report are small, compared to those with hydrogen PEMFCs, the conversion of propane will also be small. As a result the gas phase concentration of propane will not change much. That is consistent with the observation in Figure 11 that, at an inlet propane mole fraction of 0.1, variations in the inlet propane flow rate only caused small changes to the performance of the DPFC.

The effect of the fuel cell operating temperature on its overall performance is shown in Figure 12. At a current density of 40 mA/cm^2, as the fuel cell operating temperature (T) increased from 373 K (100°C) to 523 K (250°C), an increase in absolute temperature of 29%, the potential difference between the fuel cell electrodes increased, from 0.35 to 0.43 V. It was

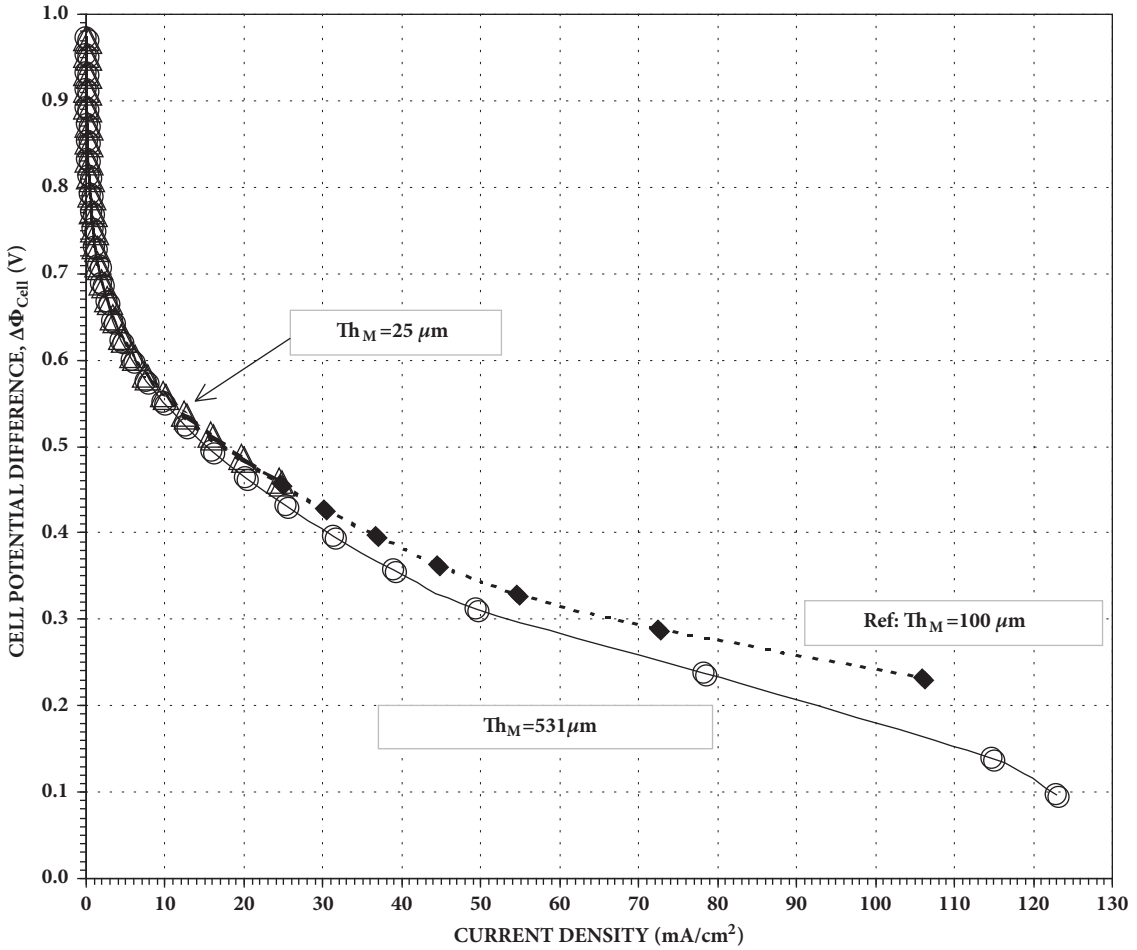

FIGURE 6: The effect of the electrolyte (membrane) layer thickness, Th_M (μm), on the polarization curve for a direct propane fuel cell (DPFC) model at 150°C and 1 atm. The values of Th_M (μm) for the above three cases were represented by the following symbols: (i) open triangles: 25 μm, (ii) solid diamonds: 100 μm (reference case), and (iii) open circles: 531 μm. All the other parameters were the same as the reference case mentioned in Table 1.

evident that temperature caused an appreciable improvement in the fuel cell performance. The potential difference between the electrodes of a fuel cell normally increases when the fuel cell operating temperature increases.

The report by Chandran et al. [38] examined fuel cell performance when the temperature increased from 40 to 60°C. In addition Ferrell et al. [45] demonstrated that fuel cell performance increased when the temperature increased from 60 to 80°C. Both those results are consistent with the increase in fuel cell performance that occurred with increasing temperature shown in Figure 12. However Ferrell et al. also performed experiments at 100°C. The fuel cell performance at 100°C was inferior to that at 80°C. The diminished performance was caused by the decrease in electrolyte membrane water content as the temperature approached the boiling point of water.

The final variables investigated were the anode and cathode total operating pressures in a DPFC. Their effect on the overall performance of the fuel cell is shown in Figure 13. At a current density of 40 mA/cm^2, as the fuel cell operating pressure (P) increased from 1 to 11 atm, the potential difference between the fuel cell electrodes increased from 0.38 to 0.71 V. From these observations, it was clear that the fuel cell total operating pressure increased the propane partial pressure and, therefore, caused a major role in enhancing the overall performance of the DPFC. This result is consistent with the work of Ferrell et al. [45] who also reported that fuel cell performance improved with increasing pressure.

The variables described above were divided into two groups. The ones related to mass transport were the membrane thickness (Figure 6), the proton conductivity (Figure 7), the proton diffusivity in the electrolyte (Figure 8), the water diffusivity in the electrolyte (Figure 9), and the propane inlet molar flow rate (Figure 11). The previous discussion indicated that all of these mass transport variables had little influence on the polarization curves.

The variables related to reaction rate were the anode exchange current density (Figure 3), the cathode exchange current density (Figure 4), the electrode layer thickness (Figure 5), the propane inlet mole fraction (Figure 10), the temperature (Figure 12), and the pressure (Figure 13). The

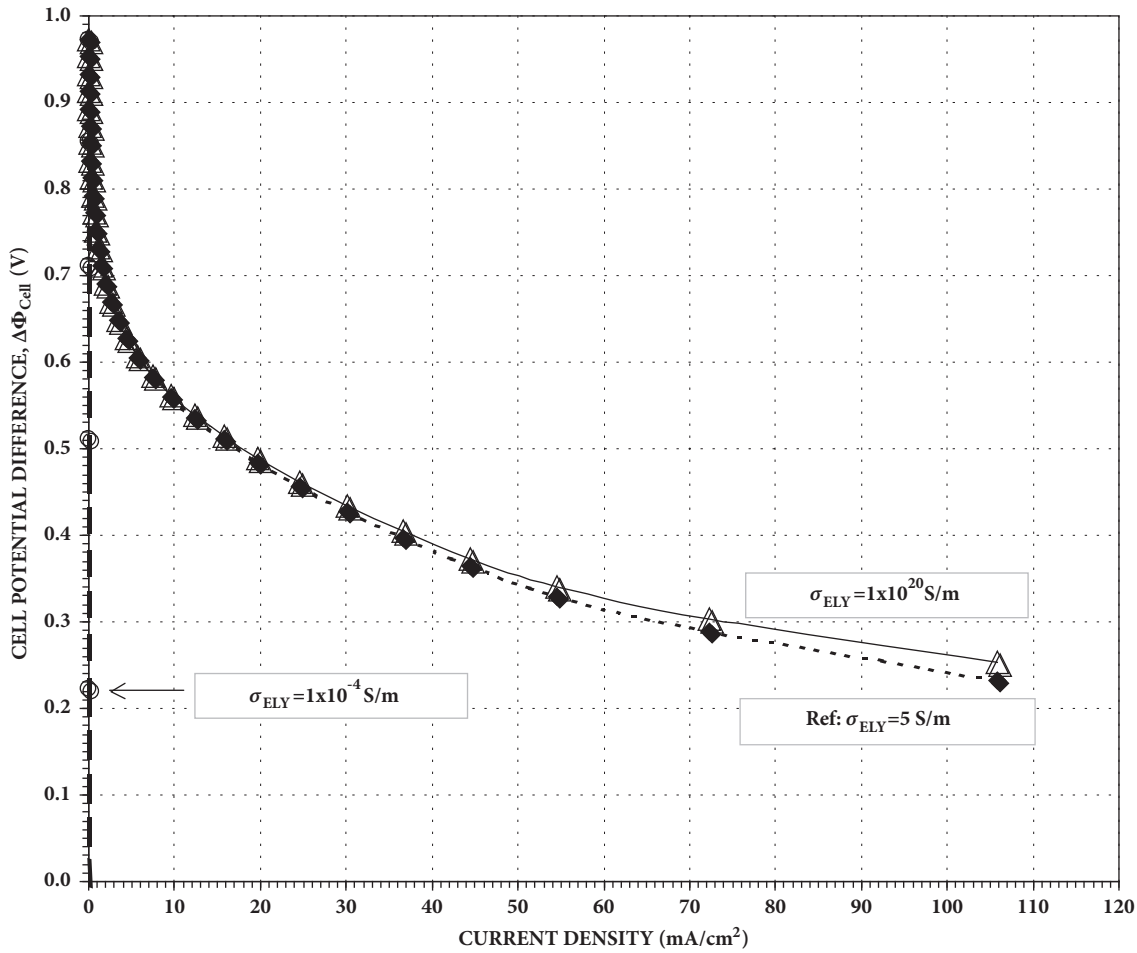

Figure 7: The effect of the membrane layer proton conductivity, σ_{ELY} (S/m), on the polarization curve for a direct propane fuel cell (DPFC) model at 150°C and 1 atm. The values of σ_{ELY} (S/m) for the above three cases were represented by the following symbols: (i) open triangles: 1x10^{20} S/m, (ii) solid diamonds: 5 S/m (reference case), and (iii) open circles: 1x10^{-4} S/m. All the other parameters were the same as the reference case mentioned in Table 1.

previous discussion indicated that all of these reaction rate variables had a significant influence on the polarization curves. Therefore mass transport appears to have little effect while reaction rate appears to have a significant effect on the polarization curves.

These results indicate that direct propane fuel cells are quite different than hydrogen PEMFCs. For hydrogen PEMFCs transport processes such as proton transport across the electrolyte and transport of oxygen through the liquid phase water at the cathode are important phenomena. For any type of fuel cell (including a DPFC) for which reaction rate is the dominant process throughout the entire polarization curve, the $\Delta\Phi_{cell}$ ordinate of the polarization curve should decrease and approach the limiting current density, j, (abscissa of the polarization curve) asymptotically. That asymptotic approach has been reported in all the experimental work on direct propane fuel cells that were reviewed in the introduction of this report. In contrast it is common for experimental polarization curves for hydrogen PEMFCs to contain a "knee" at larger current densities where an almost horizontal slope changes to an almost vertical slope, as the limiting current density is approached. The "knee" is normally caused by a change in the oxygen transport mechanism through the cathode diffusion layer.

Reaction rate phenomena are dominant up to approximately 100 mA/cm^2 in both DPFCs and hydrogen PEMFCs. The difference is that DPFCs are near their limiting current density at 100 mA/cm^2. In contrast, hydrogen PEMFCs often have limiting current densities in excess of 2000 mA/cm^2. For hydrogen PEMFCs, phenomena other than the reaction rate are dominant in the region of current density between 100 and 2000 mA/cm^2.

The results of this investigation indicate that adjusting the reaction rate variables appropriately should improve DPFC performance. However, there are some limitations. An inlet propane mole fraction of 1.0 cannot be exceeded. Species transport could become limiting if the thickness of catalyst layers is increased too much. A large increase in temperature would eliminate the advantage of rapid start-up that comes with low temperature fuel cells. Large pressures are also undesirable. In contrast anode catalyst composition, or anode exchange current density, there are variables that

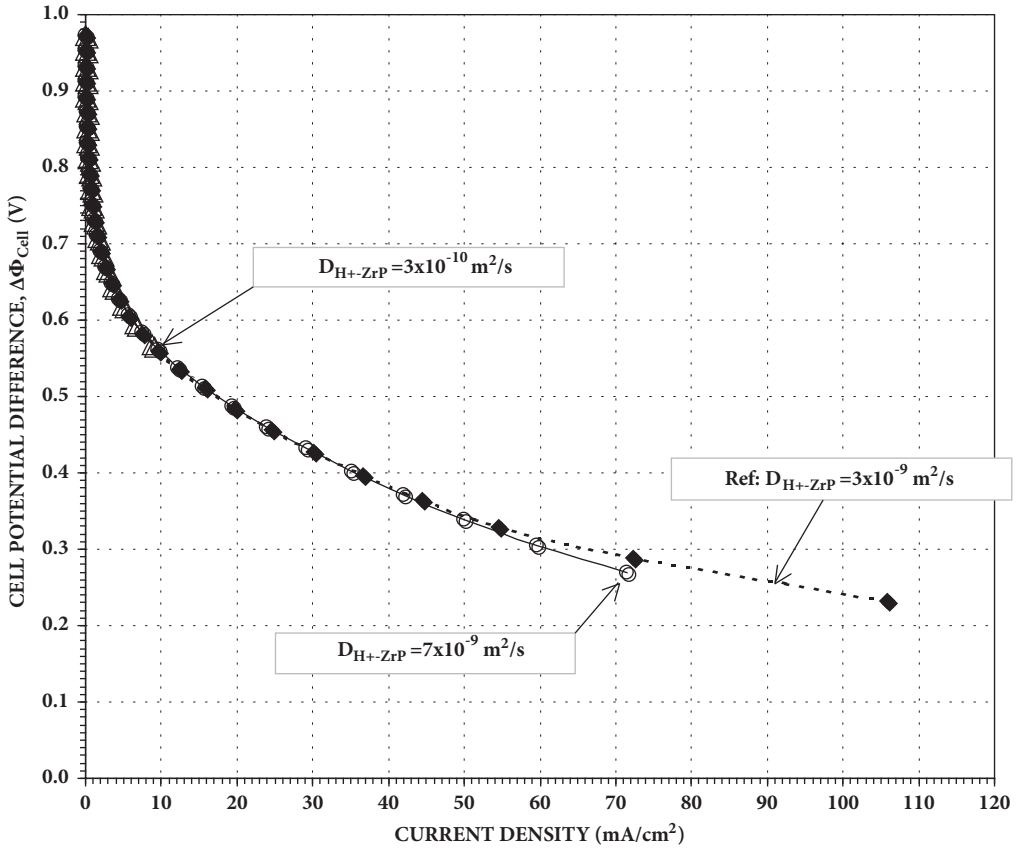

FIGURE 8: The effect of the proton diffusivity coefficient in the electrolyte phase, D_{H+-ZrP} (m^2/s), on the polarization curve for a direct propane fuel cell (DPFC) model at 150°C and 1 atm. The values of D_{H+-ZrP} (m^2/s) for the above three cases were represented by the following symbols: (i) open triangles: $3x10^{-10}$ m^2/s, (ii) solid diamonds: $3x10^{-9}$ m^2/s (reference case), and (iii) open circles: $7x10^{-9}$ m^2/s. All the other parameters were the same as the reference case mentioned in Table 1.

could have a greater impact without negative side effects. As noted earlier in this report, the performance of SOFCs fed with methane improved substantially when the methane was converted to hydrogen in a catalyst layer that preceded the layer where the electrochemical reaction of hydrogen molecules to protons occurred. In DPFCs there are several chemical reactions that precede the electrochemical reaction [9]. They include water dissociation, dehydrogenation, carbon–carbon bond cleavage, and hydroxylation. In principle, catalysts for those reactions could be added near the catalyst layer used for the hydrogen to proton electrochemical reaction.

4. Conclusions

Mass transport appeared to have little effect while reaction rate appeared to have a significant effect on DPFC polarization curves. In at least one way, DPFCs were found to be different than hydrogen PEMFCs. For DPFCs, the surface reaction rate is the dominant process for the entire polarization curve. In contrast, for hydrogen PEMFCs, the dominant phenomenon changes from reaction rate to migration of protons through the electrolyte to oxygen transport through the cathode diffusion layer, as the current density increases. However, hydrogen PEMFCs are able to operate at much larger current densities than direct hydrocarbon PEMFCs. At the same small absolute values of current densities, surface reaction rate phenomena are dominant in both types of fuel cells. Finally there is some indication in the literature that alternate catalyst compositions that have more favorable exchange current densities in direct hydrocarbon fuel cells may be found.

Nomenclature

A_{Pt}: Platinum surface area per catalyst volume (m^2_{Pt} $m^{-3}_{catalyst}$)
B': Composition-dependent transport parameter described by Khakdaman et al. [31]
c: Molar concentration of mixture (kmol m^{-3})
c_i: Molar concentration of species *i* (kmol m^{-3})

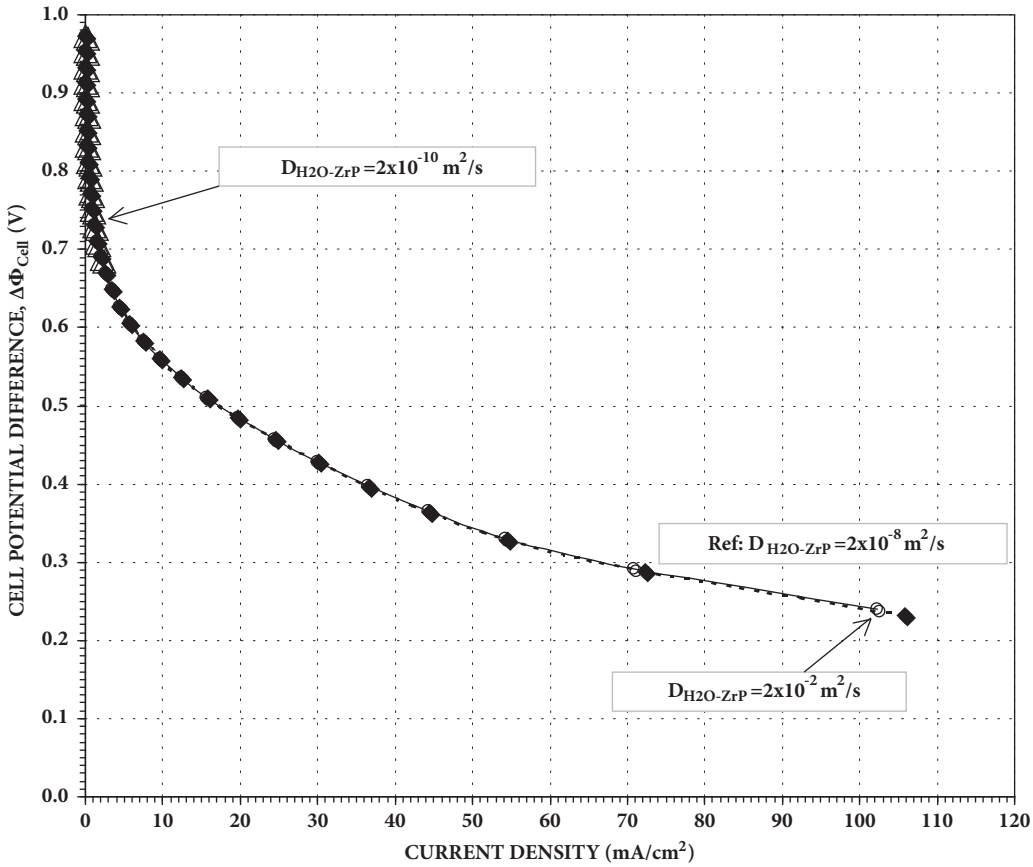

Figure 9: The effect of the water diffusivity coefficient in the electrolyte phase, $D_{H2O\text{-}ZrP}$ (m^2/s), on the polarization curve for a direct propane fuel cell (DPFC) model at 150°C and 1 atm. The values of $D_{H2O\text{-}ZrP}$ (m^2/s) for the above three cases were represented by the following symbols: (i) open triangles: $2x10^{-10}$ m^2/s, (ii) solid diamonds: $2x10^{-8}$ m^2/s (reference case), and (iii) open circles: $2x10^{-2}$ m^2/s. All the other parameters were the same as the reference case mentioned in Table 1.

D_i: Diffusion coefficient of species *i* in the gas mixture ($m^2\ s^{-1}$)

D_i: Diffusion coefficient of ion *i* in a solution ($m^2\ s^{-1}$)

D_p: Effective particle diameter (μm)

F: Faraday's constant, 96485 ($C\ mol^{-1}_{charge}$)

$(\Delta G)^{\pm}$: Activation energy for the exchange current density ($kJ\ kmol^{-1}$)

j: Volumetric current density; rate of production of proton in electrodes ($A\ m^{-3}_{catalyst}$)

j^0: Exchange current density at operating conditions ($A\ m^{-2}_{Pt}$)

$(j)^{0ref}$: Reference exchange current density at the reference conditions ($A\ m^{-2}_{Pt}$)

m: Molar flow rate ($mol\ s^{-1}$)

MW_i: Molecular weight of species *i* ($kg\ mol^{-1}$)

n: Number of species

p_i: Partial pressure of species *i* (kPa)

P: Total pressure (kPa)

PTFE: Polytetrafluoroethylene

R: Universal gas constant, 8.314 ($kJ\ kmol^{-1}\ K^{-1}$)

T: Temperature

Th: Thickness of catalyst layers and membrane (μm)

u: Superficial velocity of gas mixture (m/s)

u_i: Mobility of ion *i* in a solution (cm^2.mol/J.s)

y_i: Mole fraction of species *i* in the gas phase

x_i: Mole fraction of species *i* in the electrolyte phase

z: Moles of transferred electrons in anode and cathode reactions ($kmol_{electrons}\ kmol^{-1}_{propane}$)

ZrP: Zirconium phosphate.

Greek Letters

α_A and α_C: Anodic and cathodic charge transfer coefficients

ε: Volume fraction

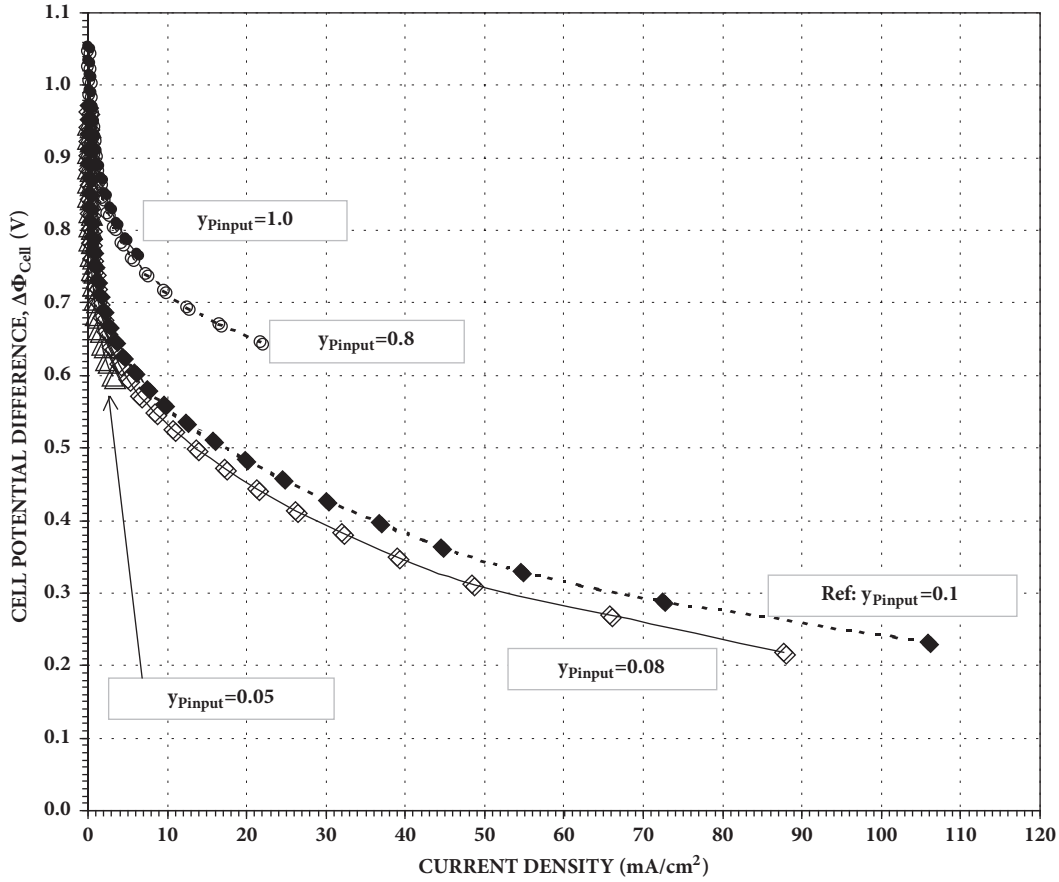

FIGURE 10: The effect of the propane inlet mole fraction, y_{Pinput}, on the polarization curve for a direct propane fuel cell (DPFC) model at 150°C and 1 atm. The values of y_{Pinput} for the above five cases were represented by the following symbols: (i) solid circles: 1, (ii) open circles: 0.8, (iii) solid diamonds: 0.1 (reference case), (iv) open diamonds: 0.08, and (v) open triangles: 0.05. All the other parameters were the same as the reference case mentioned in Table 1.

η: Overpotential (V)
μ: Dynamic viscosity (kg m^{-1} s^{-1})
ν_i: Stoichiometric coefficient of species i, positive for reactants and negative for products
ρ: Mass density (kg m^{-3})
ϕ: Electrical potential (V)
$[\phi_{Pt}]^{EQ}$: Equilibrium potential of catalyst phase (V)
$[\phi_{EYL}]^{EQ}$: Equilibrium potential of electrolyte phase (V)
$\Delta\phi$: Potential difference (Volt)
σ: Proton conductivity (S/m).

Subscripts and Superscripts

A: Anode
C: Cathode
C_3: Propane
ELY: Electrolyte
EQ: Equilibrium state
G: Gas mixture
H^+: Proton
i: Species in gas or solid phase; propane, water, CO_2, O_2, H^+ and ZrP
M: Membrane electrolyte
Pt: Platinum catalyst
ref: Reference conditions
ZrP: Zirconium phosphate in the electrolyte phase.

Data Availability

The data used to support the findings of this study are included within the article.

Conflicts of Interest

The authors declare that there are no conflicts of interest regarding the publication of this article.

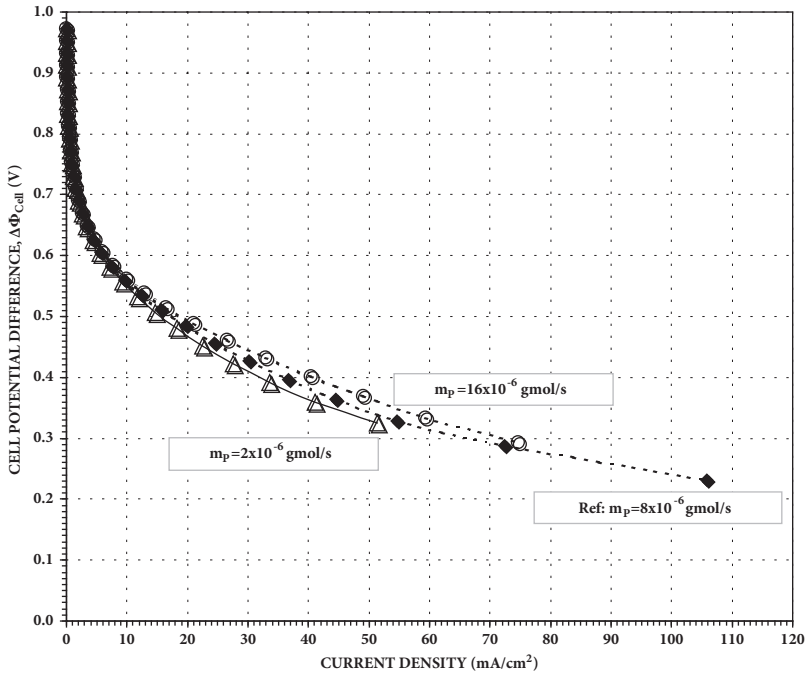

FIGURE 11: The effect of the propane inlet molar flow rate, m_P (gmol/s), on the polarization curve for a direct propane fuel cell (DPFC) model at 150°C and 1 atm. The values of m_P (gmol/s) for the above three cases were represented by the following symbols: (i) open circles: 16x10^{-6} gmol/s, (ii) solid diamonds: 8x10^{-6} gmol/s (reference case), and (iii) open triangles: 2x10^{-6} gmol/s. All the other parameters were the same as the reference case mentioned in Table 1.

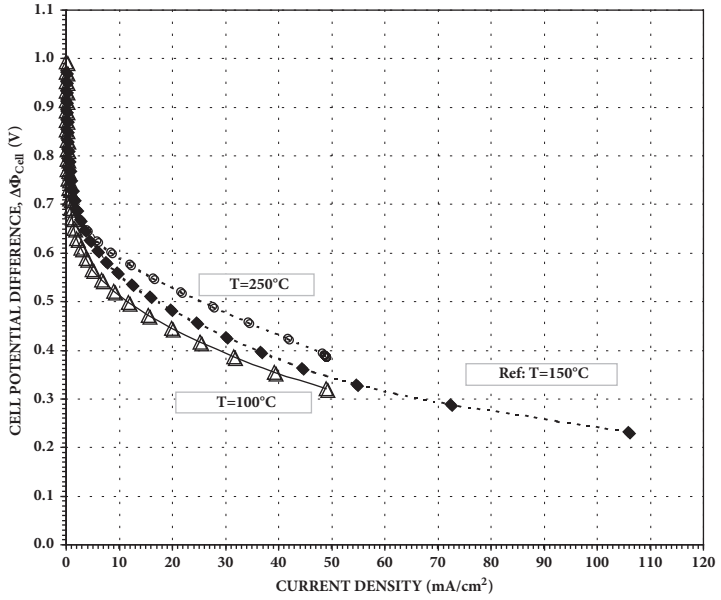

FIGURE 12: The effect of the fuel cell operating temperature, T (°C), on the polarization curve for a direct propane fuel cell (DPFC) model at 1 atm. The values of T (°C) for the above three cases were represented by the following symbols: (i) open circles: 250°C, (ii) solid diamonds: 150°C (reference case), and (iii) open triangles: 100°C. All the other parameters were the same as the reference case mentioned in Table 1.

Acknowledgments

Financial assistance is gratefully acknowledged. A Discovery grant was awarded by the Canadian Federal Government's Natural Sciences and Engineering Research Council (grant RGPIN-2015-05300). A Clean Rail grant was awarded by Transport Canada, a department within the Canadian Federal Government.

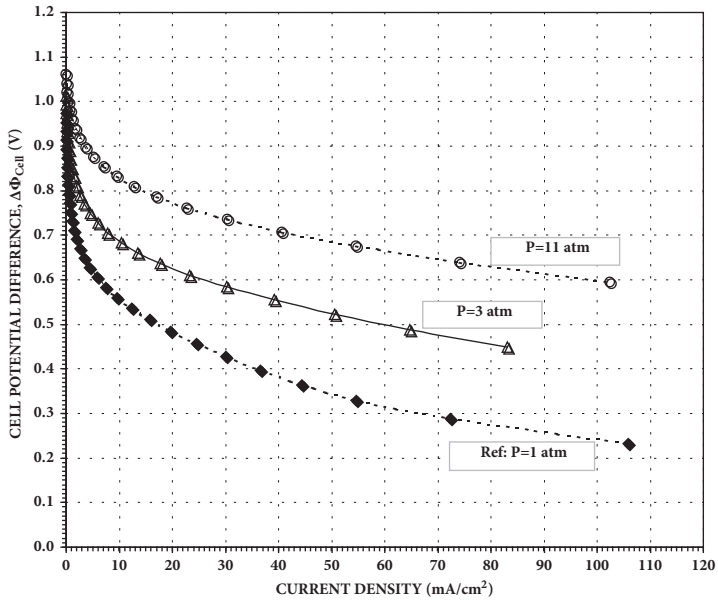

Figure 13: The effect of the fuel cell operating pressure, P (atm), on the polarization curve for a direct propane fuel cell (DPFC) model at 150°C. The values of P (atm) for the above three cases ($y_{water}/y_{propane}$ = 0.9/0.1) were represented by the following symbols: (i) open circles: 11 atm, (ii) open triangles: 3 atm, and (iii) solid diamonds: 1 atm (reference case). All the other parameters were the same as the reference case mentioned in Table 1.

References

[1] W. R. Grove, "On voltaic series and the combination of gases by platinum , Philosophical Magazine," *London*, vol. 4, pp. 127–129, 1845.

[2] M. L. Perry and T. F. Fuller, "A historical perspective of fuel cell technology in the 20th century," *Journal of The Electrochemical Society*, vol. 149, no. 7, pp. S59–S67, 2002.

[3] M. Eisler, "Getting power to the people: Technological dramaturgy and the quest for the electrochemical engine," *History and Technology*, vol. 25, no. 1, pp. 49–68, 2009.

[4] J. O. M. Bockris and S. Srinivasan, *Fuel cells: Their electrochemistry*, McGraw-Hill, New York, NY, USA, 1969.

[5] W. R. Grove, "On the Gas Voltaic Battery. Voltaic Action of Phosphorus, Sulphur and Hydrocarbons," *Philosophical Transactions of the Royal Society A: Mathematical, Physical & Engineering Sciences*, vol. 135, no. 0, pp. 351–361, 1845.

[6] J. A. A. Katelaar, "History," in *Fuel Cell Systems*, L. J. M. J. Blomen and M. N. Mugerwa, Eds., Plenum Press, New York, NY, USA, 1993.

[7] H. A. Liebhafsky and E. J. Cairns, "Direct hydrocarbon fuel cell with aqueous electrolytes," in *in Fuel Cells and Fuel Batteries*, pp. 458–523, John Wiley and Sons, New York, NY, USA, 1968.

[8] E. J. Cairns, "Anodic oxidation of hydrocarbons and the hydrocarbon fuel cell," *Advances in Electrochemical Sciences and Engineering*, vol. 8, pp. 337–391, 1972.

[9] Y. Zhu, A. Y. Tremblay, G. A. Facey, and M. Ternan, "Petroleum Diesel and Biodiesel Fuels Used in a Direct Hydrocarbon Phosphoric Acid Fuel Cell," *Journal of Fuels*, vol. 2015, pp. 1–9, 2015.

[10] J. G. Lee, O. S. Jeon, H. J. Hwang et al., "Durable and High-Performance Direct-Methane Fuel Cells with Coke-Tolerant Ceria-Coated Ni Catalysts at Reduced Temperatures," *Electrochimica Acta*, vol. 191, pp. 677–686, 2016.

[11] M. Liu, Y. Choi, L. Yang et al., "Direct octane fuel cells: A promising power for transportation," *Nano Energy*, vol. 1, no. 3, pp. 448–455, 2012.

[12] Y. Zhang, F. Yu, X. Wang, Q. Zhou, and J. Liu, "Direct operation of Ag based solid oxide fuel cells on propane," *Journal of Power Sources*, vol. 366, no. 1, pp. 56–64, 2017.

[13] W. T. Grubb and C. J. Michalske, "A High Performance Propane Fuel Cell Operating in the Temperature Range of 150◦–200◦C," *Journal of The Electrochemical Society*, vol. 111, no. 9, pp. 1015–1019, 1964.

[14] E. J. Cairns, "Hydrocarbon Fuel Cells with Fluoride Electrolytes," *Journal of The Electrochemical Society*, vol. 113, no. 11, pp. 1200–1204, 1966.

[15] O. Savadogo and F. J. Rodriguez Varela, "Low-temperature direct propane polymer electrolyte membranes fuel cell (DPFC)," *Journal of New Materials for Electrochemical Systems*, vol. 4, no. 2, pp. 93–97, 2001.

[16] C. K. Cheng, J. L. Luo, K. T. Chuang, and A. R. Sanger, "Propane fuel cells using phosphoric-acid-doped polybenzimidazole membranes," *The Journal of Physical Chemistry B*, vol. 109, no. 26, pp. 13036–13042, 2005.

[17] M. W. Verbrugge and R. F. Hill, "Experimental and theoretical investigation of perfluorosulfonic acid membranes equilibrated with aqueous sulfuric acid solutions," *The Journal of Physical Chemistry C*, vol. 92, no. 23, pp. 6778–6783, 1988.

[18] T. E. Springer, T. A. Zawodzinski, and S. Gottesfeld, "Polymer electrolyte fuel cell model," *Journal of The Electrochemical Society*, vol. 138, no. 8, pp. 2334–2342, 1991.

[19] D. M. Bernardi and M. W. Verbrugge, "A Mathematical Model of the Solid-Polymer-Electrolyte Fuel Cell," *Journal of The Electrochemical Society*, vol. 139, no. 9, pp. 2477–2491, 1992.

[20] J. Kim, S.-M. Lee, S. Srinivasan, and C. E. Chamberlin, "Modeling of proton exchange membrane fuel cell performance with an empirical equation," *Journal of The Electrochemical Society*, vol. 142, no. 8, pp. 2670–2674, 1995.

[21] J. C. Amphlett, R. M. Baumert, R. F. Mann, B. A. Peppley, and P. R. Roberge, "Performance modeling of the Ballard Mark IV solid polymer electrolyte fuel cell I. Mechanistic model development," *Journal of the Electrochemical Society*, vol. 142, no. 1, pp. 1–8, 1995.

[22] A. Z. Weber and J. Newman, "Transport in polymer-electrolyte membranes: II. Mathematical model," *Journal of The Electrochemical Society*, vol. 151, no. 2, pp. A311–A325, 2004.

[23] A. Jarauta and P. Ryzhakov, "CHAllenges in Computational Modeling of Two-Phase TRAnsport in POLymer Electrolyte Fuel CELls FLOw CHAnnels: A Review," *Archives of Computational Methods in Engineerin: State-of-the-Art Reviews*, vol. 25, no. 4, pp. 1027–1057, 2018.

[24] U. R. Salomov, E. Chiavazzo, M. Fasano, and P. Asinari, "Pore- and macro-scale simulations of high temperature proton exchange fuel cells – HTPEMFC – and possible strategies for enhancing durability," *International Journal of Hydrogen Energy*, vol. 42, no. 43, pp. 26730–26743, 2017.

[25] G. Zhang and K. Jiao, "Multi-phase models for water and thermal management of proton exchange membrane fuel cell: A review," *Journal of Power Sources*, vol. 391, pp. 120–133, 2018.

[26] G. Psofogiannakis, Y. Bourgault, B. E. Conway, and M. Ternan, "Mathematical model for a direct propane phosphoric acid fuel cell," *Journal of Applied Electrochemistry*, vol. 36, no. 1, pp. 115–130, 2006.

[27] H. Khakdaman, *A two dimensional model of a direct propane fuel cell with an interdigitated flow field [Ph.D. thesis]*, University of Ottawa, 2012.

[28] H. Khakdaman, Y. Bourgault, and M. Ternan, "A Mathematical Model of a Direct Propane Fuel Cell," *Journal of Chemistry*, vol. 2015, 2015.

[29] V. Danilov, P. De Schepper, and J. Denayer, "A TSR model for direct propane fuel cell with equilibrium adsorption and desorption processes," *Journal of Renewable Energy*, vol. 83, pp. 1084–1096, 2015.

[30] J. O. M. Bockris and S. Srinivasan, "Thermodynamic Aspects of Electrochemical Conversion," in *Fuel cells: Their Electrochemistry*, pp. 144–175, McGraw-Hill, New York, NY, USA, 1969.

[31] A. Al-Othman, A. Y. Tremblay, W. Pell et al., "A modified silicic acid (Si) and sulphuric acid (S)-ZrP/PTFE/glycerol composite membrane for high temperature direct hydrocarbon fuel cells," *Journal of Power Sources*, vol. 224, pp. 158–167, 2013.

[32] G. Psofogiannakis, A. St-Amant, and M. Ternan, "Methane oxidation mechanism on Pt(111): a cluster model DFT study," *The Journal of Physical Chemistry B*, vol. 110, no. 48, pp. 24593–24605, 2006.

[33] J. O. M. Bockris and S. Srinivasan, "Electrocatalysis," in *Fuel Cells: Their Electrochemistry*, p. 290, McGraw-Hill, New York, NY, USA, 1969.

[34] E. S. Davydova, S. Mukerjee, F. Jaouen, and D. R. Dekel, "Electrocatalysts for Hydrogen Oxidation Reaction in Alkaline Electrolytes," *ACS Catalysis*, vol. 8, no. 7, pp. 6665–6690, 2018.

[35] S. Vafaeyan, A. St-Amant, and M. Ternan, "Nickel alloy catalysts for the anode of a high temperature pem direct propane fuel cell," *Journal of Chemistry*, vol. 2014, Article ID 151638, 8 pages, 2014.

[36] Y.-J. Wang, W. Long, L. Wang et al., "Unlocking the door to highly active ORR catalysts for PEMFC applications: Polyhedron-engineered Pt-based nanocrystals," *Energy & Environmental Science*, vol. 11, no. 2, pp. 258–275, 2018.

[37] J. Liang, Z. Miao, F. Ma et al., "Enhancing oxygen reduction electrocatalysis through tuning crystal structure: Influence of intermetallic MPt nanocrystals," *Chinese Journal of Catalysis*, vol. 39, no. 4, pp. 583–589, 2018.

[38] P. Chandran, A. Ghosh, and S. Ramaprabhu, "High-performance Platinum-free oxygen reduction reaction and hydrogen oxidation reaction catalyst in polymer electrolyte membrane fuel cell," *Scientific Reports*, vol. 8, no. 1, 2018.

[39] Z. Liu, L. Ma, J. Zhang, K. Hongsirikarn, and J. G. Goodwin, "Pt alloy electrocatalysts for proton exchange membrane fuel cells: a review," *Catalysis Reviews - Science and Engineering*, vol. 55, no. 3, pp. 255–288, 2013.

[40] M. Kiani, J. Zhang, Y. Luo et al., "Recent developments in electrocatalysts and future prospects for oxygen reduction reaction in polymer electrolyte membrane fuel cells," *Journal of Energy Chemistry*, 2018.

[41] D. C. Higgins and Z. Chen, "Recent progress in non-precious metal catalysts for PEM fuel cell applications," *The Canadian Journal of Chemical Engineering*, vol. 91, no. 12, pp. 1881–1895, 2013.

[42] M. Darab, A. O. Barnett, G. Lindbergh, M. S. Thomassen, and S. Sunde, "The Influence of Catalyst Layer Thickness on the Performance and Degradation of PEM Fuel Cell Cathodes with Constant Catalyst Loading," *Electrochimica Acta*, vol. 232, pp. 505–516, 2017.

[43] S. C. DeCaluwe, A. M. Baker, P. Bhargava, J. E. Fischer, and J. A. Dura, "Structure-property relationships at Nafion thin-film interfaces: Thickness effects on hydration and anisotropic ion transport," *Nano Energy*, vol. 46, pp. 91–100, 2018.

[44] S. M. J. Zaidi, "Research trends in polymer electrolyte membranes for PEMFC," in *Polymer Membranes for Fuel Cells*, T. Matsuura and S. M. J. Zaidi, Eds., pp. 7–25, Springer, Weinheim, Federal Republic of Gemany, 2009.

[45] S. J. R. Ferrell III, T. A. Strobel, G. Gopalakrishan et al., "Exploring the fuel cell Limits of direct oxidation proton exchange membrane fuel cells with platinum based electrocatalysts," *Journal of the Electrochemistry Society*, vol. 159, no. 4, pp. B371–B377, 2012.